The mechanism of Tm to Ho energy transfer in $LiYF_4$

1992 J. Phys.: Condens. Matter 4 8525

(http://iopscience.iop.org/0953-8984/4/44/014)

J. Phys.: Condens. Matter 4 (1992) 8525–8542. Printed in the UK

The mechanism of Tm → Ho energy transfer in $LiYF_4$

Stephen A Payne, Larry K Smith, Wayne L Kway, John B Tassano and William F Krupke

University of California, Lawrence Livermore National Laboratory, PO Box 5508, Livermore, CA 94550, USA

Received 9 March 1992, in final form 27 July 1992

Abstract. The energy transfer properties of Tm, Ho:$LiYF_4$ are examined, and special attention is given to the Tm($^3F_4$) → Ho($^5I_7$) transfer dynamics and equilibration. The measured transfer times are compared with the values calculated on the basis of the static Forster–Dexter and the migration-assisted Burshtein energy transfer models (which require only spectral information and rare-earth concentrations as input data). The detection of anomalously fast measured transfer rates at high Tm doping levels is interpreted within the context of percolation theory, since migration pathways from the excited Tm ion to a Ho ion must necessarily exist above a particular threshold concentration. Lastly, it is suggested that the use of low Tm concentrations below the percolation threshold may serve to minimize the Auger upconversion losses, and also will shift the excited-state equilibrium to the Ho population; this type of scenario requires that the Tm ions be pumped directly into the $^3F_4$ state with 1.68 μm InGaAs diode sources.

1. Introduction

Solid-state lasers based on the Ho^{3+} ion have demonstrated useful performance in the 2.1 μm range. The key to the practical utility of these systems involves the co-doping of the Ho^{3+} laser ions with one or more sensitizer species. The original sensitization schemes that were devised are the so-called $\alpha\beta$-YLF ($LiYF_4$) and $\alpha\beta$-YAG ($Y_3Al_5O_{12}$) crystals [1, 2], where both Er^{3+} and Tm^{3+} are co-doped with Ho^{3+}. Because of the numerous metastable levels of the three rare-earth ions, it turns out that the dynamics of these systems are quite complicated, and that the existence of several detrimental upconversion processes causes these triply doped crystals to have lower laser efficiency than anticipated. More recently, several other systems have been actively pursued: the flashlamp-pumped Cr, Tm, Ho:YAG (CTH:YAG) laser [3], and diode laser-pumped Tm, Ho:YAG [4] and Tm, Ho:YLF [5].

The energy transfer dynamics of the sensitized Ho lasers are crucial to the effective operation of these systems. In all practical lasers currently of interest, the $^3H_4$ level of Tm^{3+} is first populated either by direct diode pumping, or by energy transfer from flashlamp-pumped Cr^{3+} ions. The Tm ions are then intended to exhibit a quantum yield near two, as illustrated in figure 1. This effect occurs because the $^3H_4$ state cross relaxes with another Tm ion to create two $^3F_4$ states [6]. Lastly, the excitation energy in the $^3F_4$ state is transferred to the $^5I_7$ upper laser level of Ho.

While most energy transfer studies have focused on the Cr → Tm step or on the cross relaxation of the Tm ions, the Tm → Ho step has not been well characterized.

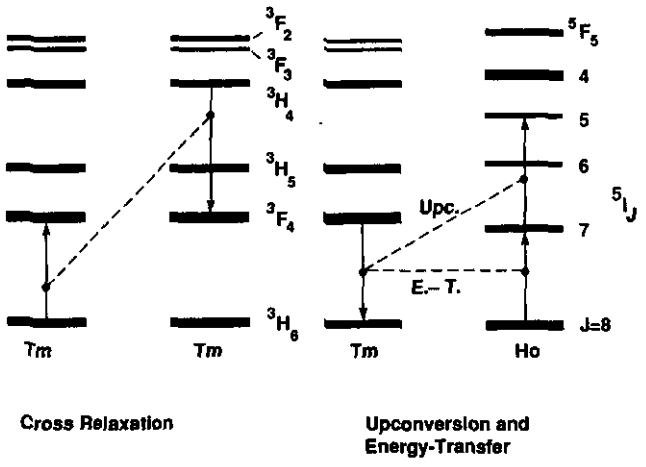

Figure 1. Energy levels of Tm and Ho, illustrating three important energy transfer processes: Tm–Tm cross relaxation leading to a quantum yield of two in the $^3F_4$ state following excitation of the $^3H_4$, energy transfer from the $^3F_4$ state of Tm to the $^5I_7$ of Ho, and Auger upconversion resulting from the interaction of Tm and Ho excited states, leading to the loss of a quantum of energy.

The Tm → Ho transfer process has been, to some extent, of less interest because it occurs so rapidly at the typical Tm concentrations that are needed to provide the quantum yield of two, noted above [7, 8]. On the other hand, the critical issues that are responsible for limiting the usefulness of the Tm-sensitized Ho laser are intimately connected with the Tm → Ho energy transfer step. One issue involves the attainment of thermal equilibrium among the $^3F_4$ and $^5I_7$ excited states of Tm and Ho, respectively, on a microsecond timescale. As a consequence of this equilibration, only the fractional population residing on the Ho ion can be extracted in a short-pulse (nanosecond) format, as is used in Q-switched oscillators and many amplifier configurations. Another crucial issue is the presence of Auger upconversion, as sketched in figure 1, where the $^3F_4$ excited state of Tm upconverts the $^5I_7$ state of Ho to the $^5I_5$, resulting in the loss of a quantum of a potential laser photon. A more precise understanding of the Tm → Ho energy transfer step may provide insight into a means of minimizing the Auger upconversion and maximizing the fractional Ho excited-state population [1–10].

In this work, we use pulsed 1.73 μm radiation to excite the Tm^{3+} ions in $LiYF_4$ directly to the $^3F_4$ state (thereby bypassing the Tm cross relaxation step), and we monitor the emissions of both Tm and Ho in order to sort out the ensuing dynamics. In addition, a continuous-wave excitation source is employed to assess the relative steady-state populations of Tm and Ho. The Forster–Dexter static transfer model [11, 12] and the Burshtein model of hopping transport [13, 14] are then utilized to calculate the energy transfer rates, based on the evaluation of the appropriate spectral overlap integrals and the rare-earth concentrations. From the comparison of these calculated results with the experimentally observed energy transfer dynamics [15], it is concluded that the regime of rapid energy migration among the Tm ions is not adequately handled within the context of these models. At this point the concept of a percolation threshold [16] in the Tm concentration is introduced, above which it is suggested that the Tm → Ho energy transfer rate becomes very rapid. It is

speculated that detrimental effects of Auger decay can be minimized by maintaining the Tm concentration below this percolation threshold. This lower Tm concentration may require that the Tm ions be diode pumped at 1.68 μm, rather than 0.8 μm. This type of pumping should be feasible with compressively strained InGaAs diodes (on the InP substrate) [17].

2. Theory of energy transfer

The two main theories of energy transfer that are commonly employed for rare-earth and transition-metal ions in insulators are that of Forster and Dexter, and of Burshtein [11–15]. The classic Forster–Dexter theory assumes sensitizers and acceptors are randomly and uniformly distributed in all of space, and that the sensitizers do not interact at all. The Burshtein model, on the other hand, includes the effect of energy migration among the sensitizer ions. The physical picture here is that the energy migrates among the sensitizers, S (Tm in our case), until it finds the acceptor ions, A (Ho).

If the sensitizer lifetime in the absence of energy transfer may be described as an exponential function with time constant τ_s, the observed decay will have the form

$$I_s(t) = I_0 \exp(-t/\tau_s) F_{F\text{-}D} F_B \tag{1}$$

where the Forster–Dexter (F-D) and Burshtein (B) decay functions have been explicitly noted in the equation. From previously published information on this topic, the functional forms may be described by

$$F_{F\text{-}D} = \exp\left(-\gamma\sqrt{t}\right) \tag{2a}$$

where the γ-parameter is given by

$$\gamma = \left(\tfrac{4}{3}\pi^{3/2} R_{SA}^3/\sqrt{\tau_s}\right) n_A \tag{2b}$$

and the critical radius R is described below. The Burshtein function may be written as

$$F_B = \exp(-\overline{W}t) \tag{3a}$$

where

$$\overline{W} = [\pi(2\pi/3)^{5/2} R_{SA}^3 R_{SS}^3/\tau_s] n_S n_A \tag{3b}$$

for the case where $R_{SA} \ll R_{SS}$, and

$$\overline{W} = [(16\pi^2/3 \times 2^{3/4}) R_{SA}^{3/2} R_{SS}^{9/2}/\tau_s] n_S n_A \tag{3c}$$

for the case where $R_{SA} \gg R_{SS}$. Here, n_S and n_A are the sensitizer and acceptor concentrations and the critical radii are given by

$$R_{SX}^6 = \frac{3c\tau_s}{8\pi^4 n^2} \int \sigma_{em}^S(\lambda)\sigma_{abs}^X(\lambda)\,d\lambda \tag{4}$$

where X = S or A, n is the refractive index, c is the speed of light, and σ_{em} and σ_{abs} are the emission and absorption spectra in cross section units for the designated species. Equations (1)–(4) will be used to calculate the energy transfer rates from the absorption and emission spectra, and these calculated rates will be compared with the actual transfer rates determined from the Tm and Ho emission decays. It should be noted that the value of the constants present in equations (3*b*) and (3*c*) is uncertain to within about a factor of two, since the precise value is found to be substantially model dependent [18, 19].

Once equilibrium between the excited states of Tm and Ho is attained, the fractional population residing with the Ho species is given by [4]:

$$f_{Ho} = n_{Ho}/\{n_{Ho} + n_{Tm}(Z_{Tm}/Z_{Ho})\exp[-(E_{Tm} - E_{Ho})/kT]\} \qquad (5)$$

where the E are the energies of the lowest crystal-field components of the $^3F_4$ and $^5I_7$ states of Tm and Ho, respectively. The partition functions are defined with

$$Z = \sum d_k \exp(-E_k/kT) \qquad (6)$$

where the energies E_k are summed over all the crystal-field components of the excited state (and the zero of energy is defined to be at the lowest component of that state).

3. Experimental methods

The Tm, Ho:$LiYF_4$ crystals studied in this work were grown by the Czochralski technique from a 2 mol% LiF-rich melt (with a 0.51/0.49 LiF/YF_3 mole ratio). Large, clear single crystals were harvested from boules having dimensions of 15–20 mm diameter × 80 mm long. These boules were generally grown free of core defects and exhibited good optical quality. The growth of these crystals was carried out by the standard Czochralski technique in a Crystalox furnace with induction heating powered by a 10 kHz generator. The melt was contained in a platinum crucible of 2 in diameter × 2 in high. The starting material used was 5–9 purity LiF, YF_3 and the rare-earth fluorides. Without pre-processing, these components in proper proportion were placed directly in the Pt crucible and melted *in situ* prior to the growth process. The melt was equilibrated at 850 °C for 12 hours to ascertain complete melting and mixing of all the components. By the use of conventional temperature control, the growth was initiated with an oriented seed and proceeded with a pull rate of 1 mm h^{-1} and a crystal rotation rate of 15 rpm. With these parameters and the properly adjusted temperature gradients, a slightly convex solid–liquid interface shape was usually maintained throughout the growth run for the size of boules mentioned above. The temperature control and the gradients were sufficiently stable such that a uniform crystal diameter was obtained without the use of additional diameter feedback controls. By slow cooling of the crystal after growth to room temperature at a rate of 100° h^{-1} the boules were all obtained in crack-free form. The crystals were oriented with the a-axis along the growth direction. The atmosphere used was high-purity nitrogen at a moderate flow rate maintained throughout the melting and growth cycle.

The main optical experiments performed in the course of this work include absorption and emission spectroscopy, and measurements of transient emission decay

[20]. The absorption cross section spectra were acquired with a Perkin–Elmer Lambda-9 spectrophotometer, along with the rare-earth concentration determination by way of the inductively coupled plasma (ICP) and mass spectrometry (MS) analytical techniques. The emission spectra were obtained by exciting the Tm ions with an Ar-ion laser-pumped DCM dye laser. The emitted photons were collected and dispersed by a McPherson 1 m monochromator before the light impinged on an InAs detector. Lock-in methods were employed to obtain a good signal-to-noise ratio, and a computer allowed for convenient manipulation of the data. A standard lamp served to correct for the spectral response of the system.

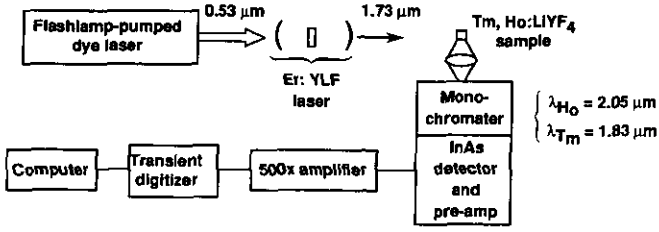

Figure 2. Experimental arrangement used to measure the $Tm(^3F_4) \rightarrow Ho(^5I_7)$ energy transfer rate. A flashlamp-pumped dye laser was employed to pump the $^4S_{3/2}$ state of Er in YLF so as to generate 1.73 μm radiation, which in turn was utilized to exclusively pump the Tm ions in the co-doped $LiYF_4$ samples. The Ho and Tm emission transients could be separately discerned by selecting the appropriate monochromator wavelength (2.05 μm for Ho, 1.83 μm for Tm).

The emission lifetimes were measured with the apparatus in figure 2. The 0.53 μm output of the flashlamp-pumped dye laser of 4 μs duration was used to pump the Er:YLF crystal in a symmetric confocal cavity in order to generate light at 1.73 μm [21]. The 1.73 μm radiation was utilized to pump the $^3F_4$ state of the Tm centres in the $LiYF_4$ sample, without directly exciting the Ho ions. The Tm or the Ho emission could be monitored with the InAs detector by selecting the appropriate wavelength with the 0.25 m monochromator. The emission decays were accumulated and averaged with a Nicolet LAS 12/70 transient digitizer, and the data were transferred to a Hewlett–Packard 87XM desktop computer for analysis.

4. Results and analyses

4.1. Calculation of transfer rates

The room-temperature σ-polarized ($E \perp c$) absorption σ_{abs} and emission σ_{em} spectra of $LiYF_4:Ho^{3+}$ and $LiYF_4:Tm^{3+}$ are displayed in the first two frames of figure 3; note that all the data are set to an absolute cross section scale. The means by which the emission cross sections were determined is discussed in our recent publication [20]. It involved the reconciliation of two methods, including the use of reciprocity with the absorption spectrum, and also the Einstein relation. On the basis of the σ-spectra in figure 3 (and the π-spectra [20] which are not shown) it is possible to calculate the overlap integrals related to the relevant critical radii, R_{SX}, of equation (4). The R_{SX} values may then be utilized to calculate the transfer rate within the context of

the Forster–Dexter (equation (2)) and Burshtein (equation (3)) models. The explicit overlap functions involve the products of absorption and emission spectra, $\sigma_{abs}\sigma_{em}$, as shown in the lower two frames. For example, the migration rate among the Tm ions is related to the $\sigma_{abs}(Tm)\sigma_{em}(Tm)$ product, yielding $R_{SS} = R_0(Tm \rightarrow Tm) = 18.4$ Å for the σ-polarization. Similarly, $R_{AA} = R_0(Ho \rightarrow Ho) = 21.7$ Å. The Tm → Ho and Ho → Tm transfer processes are related to the $\sigma_{em}(Tm)\sigma_{abs}(Ho)$ and $\sigma_{em}(Ho)\sigma_{abs}(Tm)$ products, respectively. It is therefore not surprising that $R_0(Tm \rightarrow Ho) = 17.3$ Å $> R_0(Ho \rightarrow Tm) = 11.8$ Å, since the long-wavelength lines are more pronounced in emission, and the short-wavelength features in absorption. A summary of the relevant critical radii is listed in table 1, including the π and σ results, as well as the appropriate averages $\frac{1}{3}(2R_0(\sigma) + R_0(\pi))$. The values of $\tau_{Tm} = 13.8$ ms and $\tau_{Ho} = 12.7$ ms from [20] were employed in these calculations.

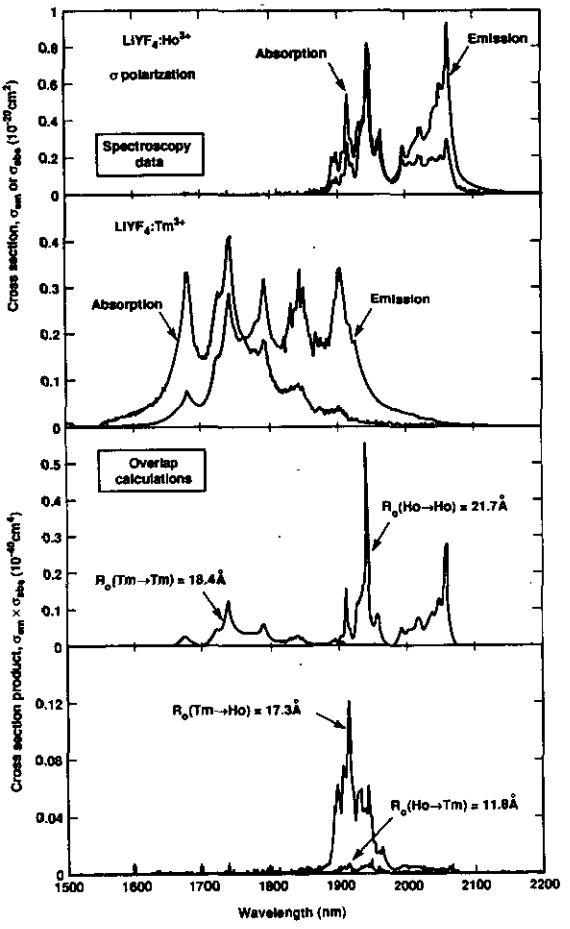

Figure 3. σ-polarized room temperature absorption and emission cross section spectra for $LiYF_4$:Ho (first frame) and $LiYF_4$:Tm (second frame). In the third frame, the overlap functions of $\sigma_{em}(Tm)\sigma_{abs}(Tm)$ and $\sigma_{em}(Ho)\sigma_{abs}(Ho)$ are shown, yielding critical radii for migration of $R_0 = 18.4$ and 21.7 Å, respectively, with the aid of equation (4). The corresponding $\sigma_{abs}(Tm)\sigma_{em}(Ho)$ and $\sigma_{abs}(Ho)\sigma_{em}(Tm)$ functions describing Tm–Ho energy transfer processes yield $R_0 = 17.3$ and 11.8 Å, and appear in the fourth frame.

Table 1. Critical radii of energy transfer processes for Tm^{3+} and Ho^{3+} in $LiYF_4$ (in Å).

Orientation	R_0(Tm → Tm)	R_0(Ho → Ho)	R_0(Tm → Ho)	R_0(Ho → Tm)
π	22.7	23.7	16.0	13.3
σ	18.4	21.7	17.3	11.8
Averaged	19.8	22.4	16.9	12.3

Now, in order to use the information in table 1 to calculate the energy transfer rates, the Tm and Ho concentrations of the $LiYF_4$ samples are needed; these measured concentrations appear in table 2 in units of 10^{19} ions cm^{-3}. The Tm dopings vary from $(0\text{–}61)\times10^{19}$ ions cm^{-3}, although the Ho concentrations fall into two groups: the lightly doped samples having $(1.2\text{–}1.3)\times10^{19}$ ions cm^{-3}, and the more highly doped samples with $(3.6\text{–}3.9)\times10^{19}$ ions cm^{-3}.

Table 2. Concentration of samples utilized in this work.

	Concentrations (10^{19} cm^{-3})	
Sample No	Tm	Ho
1	0	3.91
2	12.6	1.25
3	12.2	3.68
4	37.2	1.32
5	61.0	1.20
6	61.0	3.64

The tabulation of data in tables 1 and 2 can be used to predict the energy transfer rates. As discussed in section 2, the two basic models include the Forster–Dexter formulation, and that of Burshtein. The impact of the two processes on the functional form of the emission decay of a Tm ion that was initially excited is

$$I_{Tm}(t) = \exp\left(-t/\tau_{Tm} - \gamma\sqrt{t} - \overline{W}t\right) \tag{7}$$

where the γ- and $\overline{W}$-parameters refer to the Tm → Ho transfer processes and the back-transfer process is not accounted for. The Forster–Dexter portion is also referred to as static energy transfer, since the energy cannot migrate among the Tm ions, but instead can only transfer to Ho. The $\sqrt{t}$ functional dependence is a consequence of the fact that the Tm ions with nearby Ho acceptors decay much more rapidly than those centres for which the acceptors happen to be far away.

The Burshtein model is based on the assumption that energy migrates randomly among the Tm ions until it is deposited onto a Ho ion. The two related models described in section 2 with equations (3*b*) and (3*c*) are based on the assumptions that R_0(Tm → Tm) > R_0(Tm → Ho), and on the inverse criterion. Since our physical circumstances are such that R_0(Tm → Tm) ~ R_0(Tm → Ho), it is not clear whether we should use equation (3*b*) or (3*c*). On the other hand, the results calculated by these two methods differ by only a factor of 2.0. We therefore arbitrarily utilize equation (3*c*) since the calculated results are closer to our experimental values. It should be emphasized that equations (3*b*) and (3*c*) are in fact only intended to provide

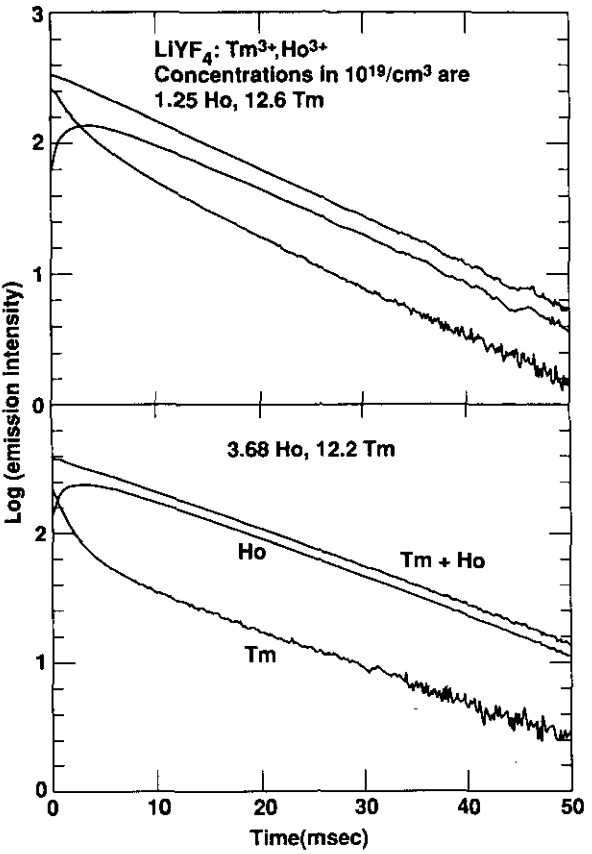

Figure 4. Room temperature emission decays of Tm and Ho for each of two samples (Nos 2 and 3 of table 2), having the concentrations noted on the figure. The curve involving the summed Tm and Ho intensities is also shown (denoted as 'Tm + Ho'). The Tm–Ho equilibration times are determined to be 3.8 and 2.0 ms and are listed in table 4. The limiting emission rates of Tm and Ho become equal after equilibration is attained.

a good estimate of the transfer rate. It is also noteworthy that both of the models predict the same linear dependence on the Tm and the Ho concentrations.

The calculated energy transfer parameters γ and $\overline{W}$ are reported in table 3. These results will be utilized shortly to calculate the characteristic Tm–Ho equilibration times.

4.2. Comparison of theoretical and measured transfer times

The room temperature emission decays of the Tm and the Ho ions are easily spectrally discriminated and are plotted in figures 4 and 5 on logarithmic intensity scales. Since the Tm ions are initially excited, the Tm decay rate (i.e., emission intensity) in figure 4 is found to decrease to a limiting rate, while the Ho emission rate is seen to increase to the same limiting value, as the Tm and Ho species come into equilibrium with each other. The Tm and Ho emission decays are adjusted so that they sum to approximately a straight line (denoted 'Tm + Ho' on the figure). Figure 4 contains

Table 3. Calculations of the Forster–Dexter and Burshtein constants for the Tm, Ho:$LiYF_4$ samples.

	Forster–Dexter ($ms^{-1/2}$)		Burshtein (ms^{-1})	
Sample No	γ(Tm → Ho)	γ(Ho → Tm)	$\overline{W}$(Tm → Ho)	$\overline{W}$(Ho → Tm)
2	0.121	0.447	0.169	0.086
3	0.355	0.432	0.484	0.245
4	0.127	1.44	0.529	0.267
5	0.116	2.16	0.788	0.400
6	0.351	2.16	2.39	1.21

the data from samples Nos 2 and 3 which have Tm contents of $\simeq 12 \times 10^{19}$ cm^{-3}, and Ho concentrations of 1.25 and 3.68×10^{19} cm^{-3}, giving evidence for energy transfer functions with $1/e$ decay times of 3.8 and 2.0 ms, respectively. Figure 5, on the other hand, displays the emission transients of samples Nos 5 and 6, which possess the high Tm dopings of 61×10^{19} cm^{-3}. Here, the transfer or equilibration times are less than 0.1 ms. The initial spike in the Tm emission decays is not due to scattered light, although this feature was not resolved as a consequence of the slow time response of the preamplifier. The short-time component may arise from nearby Tm–Ho pairs, although additional experiments are needed to confirm this. (Note that data obtained for the four samples in figures 4 and 5 each give different limiting decay times. This effect is most likely a result of quenching by unidentified impurities inadvertently incorporated into the $LiYF_4$ crystals. This quenching effect is consistently much slower than the energy transfer rate, and therefore will not have any impact on our interpretation of the data. Also note that the small dip following the short-time component is probably an electronic artifact.)

The equilibration times, τ_{eq}, derived from figures 4 and 5 are listed in table 4. The value $\tau_{eq} = 0.5$ ms for sample No 3 (not displayed) is also recorded in the table. Furthermore, we include the data reported in [22] involving a sample that contains 7.9×10^{20} Tm ions cm^{-3} and 7.9×10^{19} Ho ions cm^{-3}, where the measured equilibration time is $\tau_{eq} = 20$ μs. The data in table 3 may be used to calculate the Tm → Ho equilibration times τ_{eq}, which are defined by

$$\tau_{eq}^{-1} = \gamma^2 + \overline{W}. \tag{8}$$

Since the Tm ions incur the initial excitation, the Tm → Ho forward rates are only considered in order to estimate the τ_{eq} values. The measured and calculated τ_{eq} are reported in table 4, and agree closely for samples Nos 2 and 3, which have the lowest Tm concentrations (12×10^{19} cm^{-3}). There is substantial disagreement for sample No 3 where $n_{Tm} = 37 \times 10^{19}$ cm^{-3}, and an even larger discrepancy for samples 5, 6 and A, containing between (61–79) $\times 10^{19}$ Tm ions cm^{-3}. It appears that the Forster–Dexter and Burshtein models adequately describe the energy transfer mechanism of the samples with low Tm content. (It is noteworthy that, in fact, the Burshtein migration-assisted energy transfer is essentially responsible for nearly all of the equilibration rate for these samples.) At this time it is also clear that a new conceptual framework is required to understand why the Burshtein–Forster–Dexter theories are inadequate when $n_{Tm} > 40 \times 10^{19}$ cm^{-3}. We believe that the origin of the divergence of theory and experiment at high Tm content can be explained by percolation theory (discussed in section 5.1).

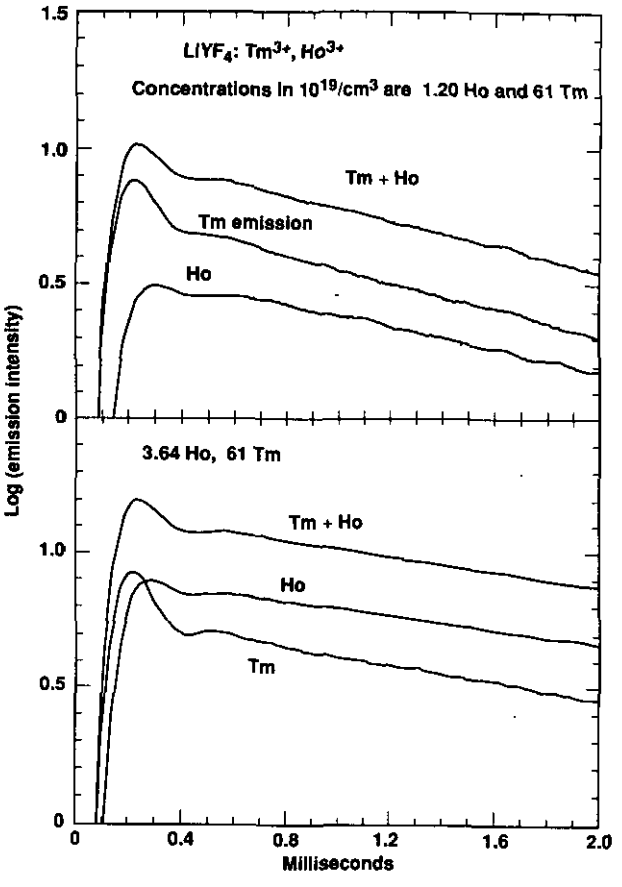

Figure 5. Room temperature emission decays of Tm and Ho for each of two samples (Nos 5 and 6 of table 2), having the rare-earth concentrations noted on the figure. The curve involving the summed Tm and Ho intensities are also shown. The Tm–Ho equilibration times are determined to be < 0.1 ms, to within the resolution of our set-up. The limiting emission rates of Tm and Ho are equal, although they are less than the values evident in figure 4, probably as a result of the presence of unidentified quenching impurities.

Table 4. Comparison of the measured and calculated properties of Tm → Ho energy transfer in YLF (sample A data taken from [22] where $n_{Tm} = 79 \times 10^{19}$ cm^{-3} and $n_{Ho} = 7.9 \times 10^{19}$ cm^{-3}).

	Equilibration time, τ_{eq}(Tm → Ho) (ms)		Fractional Ho population, f_{Ho}	
Sample No	Measured	Calculated	Measured	Calculated
2	3.8	3.4	0.62	0.75
3	2.0	1.6	0.84	0.90
4	0.5	1.8	—	0.52
5	<0.1	1.2	0.36	0.37
6	<0.1	0.4	0.63	0.64
A	0.02	0.15	—	0.75

4.3. Equilibrium among the exited-state populations

The last experimental data to be addressed relate to the Ho and Tm excited-state populations that exist after equilibrium is attained. In these room temperature experiments the Tm ions were excited near 681 nm and the π-polarized infrared emission spectrum was recorded, as is shown in figure 6 for four of the samples; the Tm and Ho concentrations are noted on the figure. By comparing these spectra with that of figure 3, it is apparent that the long- and short-wavelength portions are due to Ho and Tm, respectively, and that the spectra overlap with one another. In order to utilize the data in figure 6 to determine the relative Tm and Ho populations, three steps must be performed. First, the non-overlapping portions of the Tm and Ho emissions (in relative units of photons $nm^{-1}\ s^{-1}$) are used, in conjunction with the spectra of the isolated species from [20], to calculate the Tm and the Ho emission areas (rates in photons s^{-1}) for the π-polarization, R_π. Next, the ratios of the emission band integrals in the π- and σ-polarizations (calculated from data in [20] again), are employed to deduce the total Tm and Ho emission rates in phonons s^{-1}, i.e., $R_{tot} = R_\pi[(R_\pi + 2R_\sigma)/R_\pi]_{corr}$. Lastly, the total emission rate of each ion is multiplied by the respective radiative lifetime to obtain a quantity that is proportional to the rare-earth excited-state population, i.e., $n^*_{Ho}/n^*_{Tm} = R_{Ho}\tau_{Ho}/R_{Tm}\tau_{Tm}$ where $\tau_{Tm} = 13.8$ ms and $\tau_{Ho} = 12.7$ ms [20]. The results from this procedure provided the fractional populations residing on the excited Ho ions, $f_{Ho} = n^*_{Ho}/(n^*_{Ho} + n^*_{Tm})$, and are reported in figure 6 and table 4. For comparison, the f_{Ho}-values were calculated using the well known methods of equilibrium mechanics embodied in equation (5), and the known energy levels of Tm and Ho in $LiYF_4$ [23, 24]; these results are also listed in table 4. The agreement for samples Nos 5 and 6 is nearly exact (0.36 versus 0.37, and 0.63 versus 0.64). Since the equilibration times are so short compared to the emission lifetimes for these crystals ($\tau_{eq} < 0.1$ ms, also in table 4), equilibrium mechanics may be used to model the fractional excited-state populations. The measured and calculated f_{Ho}-results are also close for samples Nos 2 and 3, although the residual difference may arise in part from the longer equilibration times characterizing these crystals—2–4 ms.

5. Discussion

This discussion will address three areas: (i) the use of percolation theory and the nature of energy transfer and migration at high Tm doping levels; (ii) the impact of Auger upconversion on the efficiency of Tm, Ho:YLF lasers; and (iii) the potential utility of an infrared diode-pumped Tm, Ho:YLF laser.

5.1. Percolation theory

As discussed above, the energy transfer rate of $LiYF_4$ doped with a Tm concentration of 61×10^{19} cm^{-3} has been judged to be anomalously fast, based on our expectations derived from the Burshtein and Forster–Dexter models. It is concluded that the mechanisms encompassed by these models do not adequately describe the physical situation existing at the high Tm doping levels. To be more precise, the three samples containing $(1.2\text{–}1.3) \times 10^{19}$ Ho ions cm^{-3} and Tm concentrations of 12.6, 37.2 and 61×10^{19} cm^{-3}, give measured equilibration times of $\tau_{eq}(meas) = 3.8$, 0.5 and < 0.1 ms. According to the Burshtein model, the equilibration times should

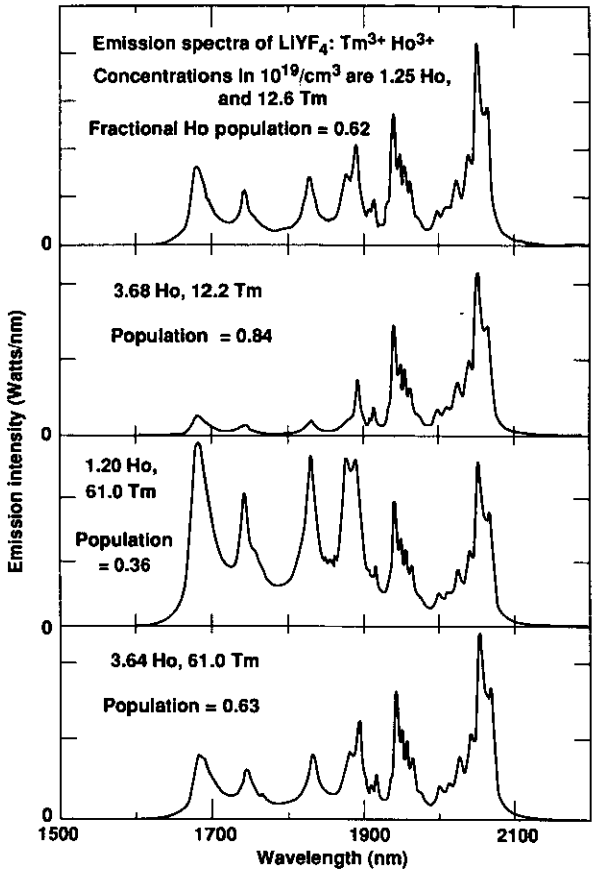

Figure 6. Room temperature π-polarized emission spectra of Tm, Ho:$LiYF_4$ obtained by exciting the Tm ions near 681 nm with a continuous-wave dye laser. These spectra are related to the equilibrium Tm–Ho excited-state population distribution and were used to determine the measured fractional populations residing on the Ho ions listed in table 4 using the prescription discussed in the text.

inversely scale with the Tm concentration, yielding $\tau_{eq}(\text{calc}) = 3.4$, 1.8 and 1.2 ms, respectively, for the three samples at hand. From the data in table 4 it appears that the rate becomes anomalously fast as the Tm doping level rises. A similar argument applies to samples Nos 3 and 6 (both contain 3.7×10^{19} Ho ions cm^{-3}). Finally, the observed rate of sample A from [22] is underestimated by a factor of 7.5 (here $n_{Tm} = 79 \times 10^{19}$ cm^{-3} and $n_{Ho} = 7.9 \times 10^{19}$ cm^{-3}). The suggestion is now introduced that once a particular threshold is reached, the excitation on any Tm ion will always be able to find a fast-migration pathway to a Ho ion. The existence of this route is very reminiscent of the percolation theory.

Percolation theory was originally discussed primarily within the context of conductivity phenomena that exhibit threshold-like behaviour, although it has now been applied to a diverse array of physical problems [16, 25, 26]. For the imagined circumstance where centres are randomly dispersed throughout space, and where conduction occurs between any two centres only if they are separated by less than distance R_{crit}, the percolation threshold concentration is given by [27]

$$n_{perc} = 2.7/(\tfrac{4}{3}\pi R_{crit}^3). \tag{9}$$

In other words, it turns out that for $n > n_{perc}$, conduction (or more generally communication) exists between centres over large distances. It is also true that nearly all of the centres tend to occur in these macroscopically connected clusters. While these concepts form the essence of percolation theory, the numerical aspects of the problem vary depending on the nature of the communication mechanism, and on the placement of the centres. The model quoted above in equation (9) has been selected among the many existing formulations to be most closely related to the physical situation at hand.

The main difficulty with equation (9) is that of selecting an appropriate value for R_{crit}. One possible way to estimate R_{crit} is to assume that the average distance migrated must correspond to the average distance between Ho ions:

$$\sqrt{N_{step}}\,R_{crit} = n_{Ho}^{-1/3} \tag{9a}$$

where the random walk model is being applied for the excitation energy taking N_{step} number of steps, each of which is R_{crit} in length. From the basic theory of energy transfer we may write that

$$N_{step} = [R_0(\mathrm{Tm} \rightarrow \mathrm{Tm})/R_{crit}]^6 . \tag{9b}$$

From tables 1 and 2 we find that $R_0(\mathrm{Tm} \rightarrow \mathrm{Tm}) = 19.8$ Å and that $n_{Ho} = 1.3 \times 10^{19}$ cm^{-3}, and with equations (9) it is calculated that $R_{crit} = 13.5$ Å. Using this value in equation (8) gives a percolation threshold of $n_{perc} = 26 \times 10^{19}$ Tm ions cm^{-3}. This exercise shows that the calculated n_{perc} is of the order of our experimental result of $\simeq 40 \times 10^{19}$ cm^{-3}, where the measured and calculated τ_{eq}-values of table 4 begin to diverge.

Since this percolation approach is probably being applied to this type of energy transfer problem for the first time, it is not highly developed yet. In fact, we have thus far only been able to provide an estimate of the percolating sensitizer concentration at which the Burshtein model will begin to fail. On the basis of our data and analysis, we predict that, as the Tm sensitizer concentration rises from low → intermediate → high, the predominating theoretical framework will progress from Forster–Dexter → Burshtein → percolation. We might qualitatively expect, however, that the energy transfer rate will become somewhat less sensitive to the magnitude of the value of $R_0(\mathrm{Tm} \rightarrow \mathrm{Ho})$ when $n_{Tm} > n_{perc}$, since the excitation energy will essentially always be able to migrate to a lattice site near to a Ho ion. This is possible since there are 32 neighbouring Y sites near to a given Ho ion, within a radius of 8.2 Å [7]. We note in passing that areas of research relating to our approach include the application of Anderson localization to ruby [28] and the concept of exciton percolation to naphthalene crystals [29, 30].

5.2. Auger upconversion in Tm, Ho:$LiYF_4$

One of the problems that adversely impacts solid-state lasers based on Tm, Ho-co-doped materials is the Auger upconversion process (see section 1 and figure 1 for a discussion of this effect). Here an excited Tm migrates to an excited Ho ion, such that excited-state–excited-state annihilation occurs; i.e., the Tm ion returns to its $^3H_6$

ground state, and the Ho is upconverted to the higher-lying $^5I_5$ excited state. The Ho then non-radiatively converts back to the $^5I_7$ state with the net result that one quantum of potential laser energy has been lost.

Auger upconversion is known to present a serious loss mechanism for Tm, Ho:YAG, and is likely to be a serious problem for YLF as well. The question is whether the impact of this dynamical loss mechanism can be mitigated in any way. The first task to be performed involves generating an estimate of the critical radius of the upconversion process. To provide this we calculated the form of three spectra: the $^3F_4 \rightarrow {}^3H_6$ emission spectrum of Tm:$LiYF_4$, the $^5I_8 \rightarrow {}^5I_7$ ground-state absorption of Ho, and the $^5I_7 \rightarrow {}^5I_5$ excited-state absorption of Ho. These simulated spectra are displayed in figure 7 and were calculated by assuming that all of the individual cross sections between each pair of crystal-field levels [23, 24] are equal. Then, after accounting for the thermal population distributions in each initial state, all of the (thermally weighted) transitions occurring within 50 cm^{-1} intervals were tallied and plotted in the figure. It is apparent that the Tm emission and the Ho ground-state absorption of figure 7 are similar to the actual spectra presented in figure 3, suggesting that our methods are based on a reasonable procedure and that the calculated Ho excited-state absorption spectrum is an acceptable rendition of the unknown actual line shape. Lastly, the ratios of the areas of the $^5I_7 \rightarrow {}^5I_5$ and $^5I_7 \rightarrow {}^5I_8$ transitions were scaled from the ratio of the Judd–Ofelt $|U^{(6)}|^2$ matrix elements (since the $U^{(4)}$- and $U^{(2)}$-elements are known to be much smaller) [31]. From the data in figure 7 and the use of equation (4) it is possible to calculate the ratio of the critical radii for the energy transfer and Auger processes, yielding

$$R_0(\text{transfer})/R_0(\text{Auger}) = 1.8. \tag{10}$$

It is noteworthy that the critical radius for energy transfer is substantially favoured over that of upconversion. By relying on the insights that we have developed concerning migration and percolation, it may be suggested that the energy transfer and upconversion processes will be maximally distinguished if the Tm concentration is maintained below the percolation threshold, where the Tm, Ho system is guided by Burshtein-type dynamics. Using equations (3*c*) and (10), and assuming that the ground and excited Ho populations are equal, gives $\overline{W}(\text{transfer})/\overline{W}(\text{Auger}) = 2.4$; equation (3*b*) gives 5.8.

The main difficulty in utilizing lower Tm concentrations is that, under the circumstances that are commonly employed for laser operation, the Tm ions are pumped near 780 nm with AlGaAs diodes, and the Tm concentration is adjusted to be $> 30 \times 10^{19}$ cm^{-3} in order that the 2-for-1 quantum yield is rendered about 90% efficient [22] (see section 1 and figure 1). Unfortunately, this required Tm concentration is so high that it allows rapid migration above the percolation threshold, thereby giving rise to an enhanced Auger upconversion rate. Since the use of higher Tm doping also causes more of the equilibrium population to reside on the Tm ions (rather than Ho), we next consider whether it is feasible to pump the $^3F_4$ state of Tm directly in the infrared at 1.68 μm, and circumvent the 2-for-1 process altogether.

5.3. Prospects for a 1.68 μm-diode-pumped Tm, Ho:YLF laser

The infrared π-polarized absorption of Tm^{3+}, and emission of Ho^{3+}, are displayed in figure 8. The Ho emission cross section of 1.84×10^{-20} cm^2 is sufficiently large to allow for efficient energy extraction in Q-switched and amplifier configurations.

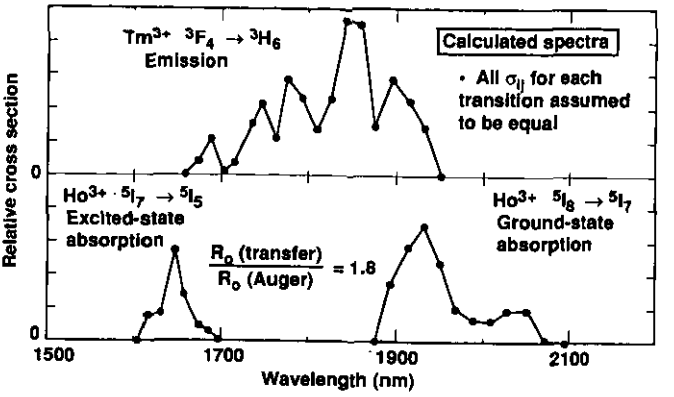

Figure 7. Calculated room temperature spectra of Tm and Ho in $LiYF_4$ (compare with figure 3), using the procedure indicated in the text. The spectral overlap of the Tm $^3F_4 \rightarrow {}^3H_6$ emission, with the Ho $^5I_7 \rightarrow {}^5I_5$ *excited-state absorption and* $^5I_8 \rightarrow {}^5I_7$ ground-state absorption, provides an estimate of ratio of the critical radii for the energy transfer and upconversion processes of 1.8.

In addition, the large Tm absorption of 1.65×10^{-20} cm^2 and the long Ho emission lifetime of 16 ms effectively permit favourable pumping conditions. One of the important disadvantages of Ho in $LiYF_4$ is that a minimum of $\beta_{min} = 24\%$ of the Ho ions must be inverted before the ground-state absorption losses are completely overcome [32].

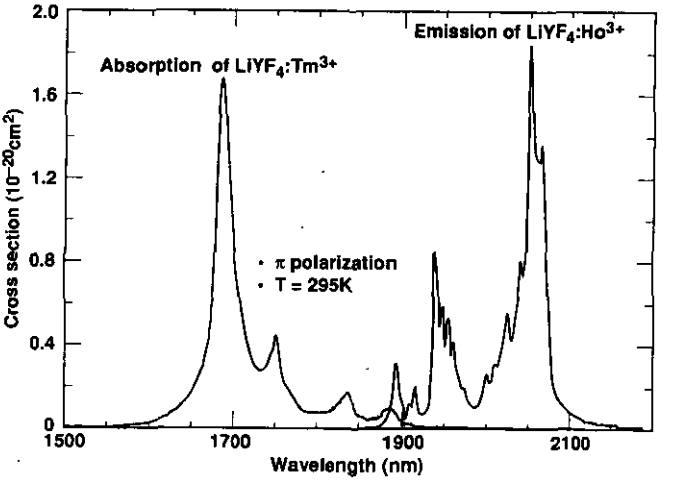

Figure 8. Room temperature π-polarized absorption spectrum of Tm, and emission spectrum of Ho in YLF, on an absolute cross section scale. The large cross sections and favourable energy transfer properties suggest that it may be useful to pump Tm at 1.68 μm with an infrared-emitting laser diode.

As noted above, the use of reduced Tm concentrations requires that the $^3F_4$ state be pumped directly at 1.68 μm. Although diodes are not normally produced

to generate this wavelength, the required device structure is closely related to the common 1.55 μm diode utilized in fibre-optic communication applications. The preferred structure required to operate at 1.68 μm involves the use of an InP substrate and a compressively strained InGaAs active region (with a somewhat more In-rich composition compared to the 1.55 μm devices) [17, 33]. Interestingly, recent evidence indicates that compressively strained InGaAs laser diodes may bear numerous advantages over the devices that are either unstrained or under tensile stress.

As an example of a Tm, Ho:YLF crystal pumped by a 1.68 μm laser diode, we consider the rare-earth concentrations employed in sample No 3, where $n_{Tm} = 12 \times 10^{19}$ cm^{-3} and $n_{Ho} = 3.6 \times 10^{19}$ cm^{-3}. An effective Ho pump saturation parameter for excitation via the Tm ions is suggested to be

$$I_{sat}^{Ho} = h\nu/[\sigma_{pump}^{Tm}\tau_{em}f_{Ho}(n_{Tm}/n_{Ho})]. \tag{11}$$

The f_{Ho} accounts for the fraction of the population residing on the Ho ions, and the n_{Tm}/n_{Ho} ratio is included to convert the Tm pump cross section into an effective value for the Ho ions. Using $\tau_{em} = 16$ ms, the $\sigma_{pump}^{Tm} = 1.65 \times 10^{-20}$ cm^2 peak absorption cross section, and taking $f_{Ho} = 0.75$ (the $f_{Ho} = 0.84$ value from table 4 was decreased to account for the partial depletion of the Ho population), we calculate that $I_{sat}^{Ho} = 0.21$ kW cm^{-2}. If the Tm, Ho:YLF laser crystal is pumped at this intensity, most of the Ho ions will be inverted (remember that at least 24% is required). Based on typical intensities available from laser diodes, the concept of a Tm, Ho:YLF laser pumped with a 1.68 μm laser diode, is judged to be reasonable.

6. Summary

The Tm($^3F_4$) $\rightarrow$ Ho($^5I_7$) energy transfer study of co-doped $LiYF_4$ reported in this paper is focused on performing all the necessary experiments and analyses required to elucidate the underlying physical mechanisms operating in the medium. The Forster–Dexter and the Burshtein models are used to calculate the energy transfer rates. These calculations are fundamentally based on evaluating the critical radii, which in turn are derived primarily from spectral overlap integrals. The careful comparison of the calculated and measured transfer rates reveals that the experimental rates become anomalously fast at higher Tm doping levels. This observation is interpreted within the context of percolation theory where, above a certain threshold sensitizer concentration, the excitation energy is always able to find a migration pathway to the Ho acceptor. Separate experiments involving continuous-wave excitation were conducted to investigate the equilibrium properties of the Tm, Ho:$LiYF_4$ crystals, and have confirmed that the fractions of Tm and Ho populations present are precisely the same as predicted from equilibrium statistical mechanics.

In order to deploy the most efficient Tm, Ho:YLF laser material, it is preferable to minimize the Tm concentration so as to shift the excited-state population to the Ho ions. In addition, reducing the Tm concentration below the percolation threshold will help to minimize the Auger upconversion loss (which is characterized by a small critical radius and is suggested to be crucially dependent on the presence of ultrafast migration). The reduced Tm concentration is best accommodated by pumping the $^3F_4$ state of Tm directly at 1.68 μm with a diode laser. An examination of the current literature indicates that this type of diode is similar to the existing 1.55 μm variety that is currently employed in fibre communication technology.

Acknowledgments

Firstly, one of us (SAP) wishes to thank Professor Richard Zallen for his expert advice on percolation theory, and its applicability to our energy transfer problem. We wish also to thank E Prochnow and R Vallene for fabricating the YLF samples, C Otto and T Duewer for the Tm and Ho concentration determinations, and T Pollak of Sanders Associates for supplying the Er:YLF crystal used in the 1.73 μm laser source. This work was performed under the auspices of the US Department of Energy by Lawrence Livermore National Laboratory under contract No W-7405-ENG-48.

References

[1] Johnson L F, Geusic J E and Van Uitert L G 1966 *Appl. Phys. Lett.* **8** 200
[2] Chicklis E P, Naiman C S, Folweiler R C and Doherty J C 1972 *IEEE J. Quantum Electron.* **QE-8** 225
[3] Quarles G J, Rosenbaum A, Marquardt C L and Esterowitz L 1989 *Appl. Phys. Lett.* **55** 1062
Bowman S R, Winings M J, Auyeung R C Y, Tucker J E, Searles S K and Feldman B J 1991 *IEEE J. Quantum Electron.* **QE-27** 2142
[4] Fan T Y, Huber G, Byer R L and Mitzscherlich 1988 *IEEE J. Quantum Electron.* **QE-24** 924
[5] Hemmati H 1989 *Opt. Lett.* **14** 435
Storm M D and Deyst J P 1991 *IEEE Trans. Photonics Technol. Lett.* **3** 982
[6] Antipenko B M, Buchenkov V A, Glebov A S, Kiseleva T I, Nikitichev A A and Pismennyi V A 1988 *Opt. Spectrosc. (USSR)* **64** 772
[7] Brenier A, Rubin J, Moncorge R and Pedrini C 1989 *J. Physique* **50** 1463
[8] Bowman S R, Winings M J, Searles S and Feldman B J 1991 *IEEE J. Quantum Electron.* **QE-27** 1129
[9] Armagan G, Buoncristiani A M and DiBartolo B 1991 *J. Lumin.* **48 & 49** 171
[10] Storm M E 1988 *Appl. Opt.* **27** 4170
[11] Dexter D L 1953 *J. Chem. Phys.* **21** 836
Forster T 1949 *Z. Naturf.* **49** 321
[12] Inokuti M and Hirayama F 1965 *J. Chem. Phys.* **43** 1978
[13] Burshtein A I 1972 *Sov. Phys.–JETP* **35** 882
[14] Voron'ko Yu K, Mamedov T G, Osiko V V, Prokhorov A M, Sakun V P and Shcherbakov I A 1976 *Sov. Phys.–JETP* **44** 251
[15] For a particularly lucid and useful rendition of the Forster–Dexter and Burshtein models, see Caird J A, Ramponi A J and Staver P R 1991 *J. Opt. Soc. Am.* B **8** 1391
[16] Zallen R 1983 *The Physics of Amorphous Solids* (New York: Wiley)
[17] Thijs T J A, Tiemeijer L F, Kuindersma P I, Binsma J J M and VanDangen T 1991 *IEEE J. Quantum Electron.* **QE-27** 1426
[18] Bondar I A, Burshtein A I, Krutikov A V, Mezentseva L P, Osiko V V, Sakun V P, Smirnov V A and Shcherbakov I A 1981 *Sov. Phys.–JETP* **54** 45
[19] Burshtein A I 1983 *Sov. Phys.–JETP* **57** 1165
[20] Payne S A, Chase L L, Smith L K, Kway W L and Krupke W F 1992 *J. Quantum Electron.* to be published
[21] Barnes N P, Allen R E, Esterowitz L, Chicklis E P, Knights M G and Jenssen H P 1986 *IEEE J. Quantum Electron.* **QE-22** 337
[22] Armagan G, Buoncristiani A M, Inge A T and DiBartolo B 1991 *OSA Proc. on Advanced Solid-State Lasers* vol 10, ed G Dubé and L Chase (Washington, DC: Optical Society of America) p 222
[23] Jenssen H P, Linz A, Leavitt R P, Morrison C A and Wortman D E 1975 *Phys. Rev.* B **11** 92
[24] Karayianis N, Wortman D E and Jenssen H P 1976 *J. Phys. Chem. Solids* **37** 675
[25] Dorenbos P, Lee V D and den Hartog H W 1988 *Phys. Rev.* B **37** 10312
[26] Dorenbos P and den Hartog H W 1989 *Phys. Rev.* B **40** 5817
[27] Fremlin D H 1976 *J. Physique* **37** 813
[28] Lyo S K 1971 *Phys. Rev.* B **3** 3331
[29] Kopelman R, Monberg E M and Ochs F W 1977 *Chem. Phys.* **21** 373

[30] Ahlgren D C, Monberg E M and Kopelman R 1979 *Chem. Phys. Lett.* **64** 122
[31] Carnall W T, Crosswhite H and Crosswhite H M 1977 Energy level structure and transition probabilities of the trivalent lanthanides in LaF_3 *Argonne National Laboratory, USA* Internal Document
[32] Chase L L and Krupke W F 1990 *Opt. Quantum Electron.* **22** S1
[33] Agrawas G P and Dutta N 1986 *Long-Wavelength Semiconductor Lasers* (New York: Van Nostrand Reinhold)